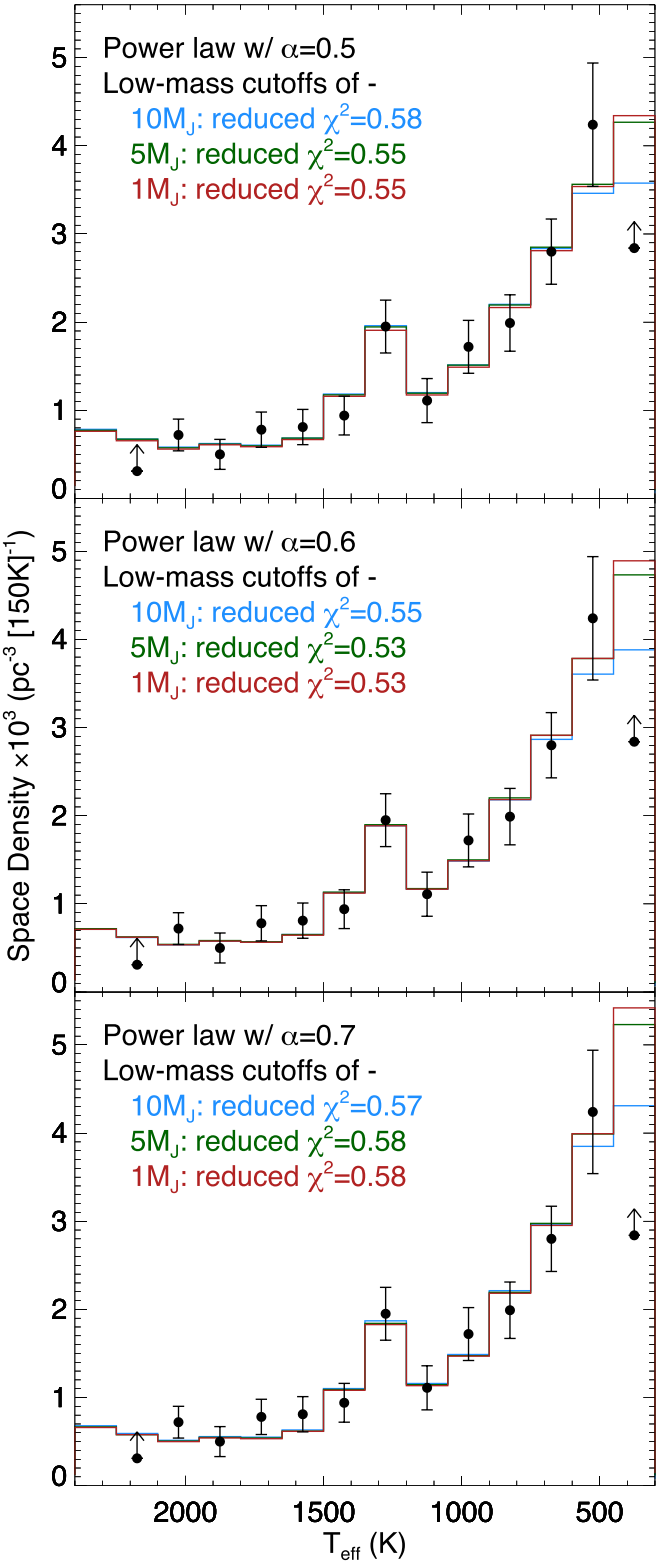

Figure 29. Fits of power laws with $\alpha = 0.5$ (top panel), $\alpha = 0.6$ (middle panel), and $\alpha = 0.7$ (bottom panel) to our observational data (black points). These predicted $T_{\rm eff}$ distributions have been passed through the evolutionary models of Saumon & Marley (2008). Each panel shows simulations for three low-mass cutoffs: 10 $M_{\rm Jup}$ (blue), 5 $M_{\rm Jup}$ (green), and 1 $M_{\rm Jup}$ (red). The minimum reduced χ^2 values are found for the $\alpha = 0.6$ model.

Baraffe et al. (2003) models, which explore even colder temperatures, we find that the mass range shrinks to $< 15 M_{\rm Jup}$ for the 150–300 K bin.)

For the warm bins with the narrowest mass distributions (2100–2250 K and 1950–2100 K), the two objects in Table 16 with dynamical measures have masses in accordance with the model predictions. Good agreement is seen at cooler bins as well. The only objects with measures that may be discrepant with expectations are the four objects in the 1650–1950 K range (Gl 564B and C, DENIS 2252+1730A, 2MASS 0700 +3157A) in panel (a), the highest-mass object in the 1200–1350 K bin (Gl 845B) along with the two objects in the 900–1050 K bin (Gl 229B and Gl 845C) of both panels, and the three lowest-mass objects (SDSS 0423−0414B and WISE 1049−5319AB) in the 1200–1350 K bin of panel (b).

These latter three objects can be explained by the inability of the older Baraffe et al. (2003) models to account for clouds in this range, since these objects do not appear unusual when compared to the expectations from Saumon & Marley (2008).

The other objects deserve closer scrutiny:

1. Gl 564BC: This pair has masses lower than 85% of objects in the 1650–1800 K bin. Objects of this mass, according to our simulations, would have a relatively young age of $\sim$580 $\pm$ 67 Myr. Potter et al. (2002) note that the primary in this system, the G2 dwarf Gl 564A, is chromospherically active, a fast rotator, and an object of high lithium abundance, which places its age at <800 Myr. After a more careful analysis, Dupuy et al. (2009) adopt an age for the primary of 790^{+220}_{-150} Myr, which accords with the young age expected by our simulations.
2. DENIS 2252−1730A: The is the third other object in the 1650–1800 K bin. It has a dynamical mass intermediate between Gl 564B and Gl 564C, and would thus be expected from our simulations to have a similarly young age. However, there does not appear to be independent verification of a young age in the literature, such as a measurement of lithium absorption in the A component (Dupuy & Liu 2017).
3. 2MASS 0700+3157A: This object falls in the 1800–1950 K bin. Our simulations find that it has a mass lower than 85% of objects in its temperature bin, implying another relatively young age of 755 $\pm$ 101 Myr. There is no independent assessment of age for this object, although Dupuy & Liu (2017) also note the model-implied young age for the primary. As stated in that work, Thorstensen & Kirkpatrick (2003) report no lithium in the joint spectrum of the AB pair, which would likely mean only that the age is >200 Myr.
4. Gl 845BC: The masses of both components are surprisingly high for their respective temperature bins. In our simulations that use the Saumon & Marley (2008) evolutionary models, we find $\sim$250,000 objects in our three-million-object simulation that fall in the 1200–1350 K bin inhabited by Gl 845B, but none of these simulated objects has a mass as high as Gl 845B. Likewise, of our $\sim$190,000 simulated objects in the 900–1050 K bin, none has a mass as high as Gl 845C. This system is not believed to be exceptionally old, either (see Dieterich et al. 2018), which might partly explain the ultra-high masses. Switching to the Baraffe et al. (2003) evolutionary code instead gives a similar result. The published mass measurements for this system are completely at odds with theoretical expectations.

Table 16
Masses for L, T, and Y Members of the 20 pc Census

Object (1)	Sp. Type (2)	$T_{\rm eff}$ (K) (3)	Mass ($M_{\rm Jup}$) (4)	Method (5)	Mass References (6)
2MASS 0045+1634	L2γ	2059 ± 45	24.98 ± 4.62	MovGp	F
WISE 0047+6803	L6-8γ	1230 ± 27	11.84 ± 2.63	MovGp	F
SIMP 0136+0933	T2	1051 ± 198	12.7 ± 1.0	MovGp	G
2MASS 0355+1133	L3-6γ	1478 ± 58	21.62 ± 6.14	MovGp	F
SDSS 0423-0414A	L6.5:	1465 ± 134	$51.6^{+1.5}_{-2.5}$	dynam	D
SDSS 0423-0414B	T2	1218 ± 79	$31.8^{+1.5}_{-1.6}$	dynam	D
AB Dor Cb(0528-6526)	···	···	14 ± 1	MovGp	C
Gl 229B(0610-2152)	T7 pec	927 ± 77	70 ± 5	dynam	A
2MASS 0700+3157A	L3:	1838 ± 134	68.0 ± 1.6	dynam	D
2MASS 0700+3157B[C]	L6.5:	1465 ± 134	$73.3^{+2.9}_{-3.0}$	dynam	D
WISE 0720-0846B	[T5.5]	1183 ± 88	66 ± 4	dynam	T
2MASS 0746+2000A	L0	2237 ± 134	$82.4^{+1.4}_{-1.5}$	dynam	D
2MASS 0746+2000B	L1.5	2029 ± 134	78.4 ± 1.4	dynam	D
WISE 1049-5319A	L7.5	1334 ± 58	$34.2^{+1.3}_{-1.1}$	dynam	V
WISE 1049-5319B	T0.5:	1261 ± 55	$27.9^{+1.1}_{-1.0}$	dynam	V
SDSS 1110+0116	T5.5	926 ± 18	10-12	MovGp	I
LHS 2397aB(1121-1313)	[L7.5]	1282 ± 88	66 ± 4	dynam	D
2MASS 1324+6358	T2: pec	1051 ± 197	11-12	MovGp	H
DENIS 1425-3650	L4γ	1535 ± 53	22.52 ± 6.07	MovGp	F
Gl 564B(1450+2354)	L4	1722 ± 134	$59.8^{+2.0}_{-2.1}$	dynam	D
Gl 564C(1450+2354)	L4	1722 ± 134	$55.6^{+2.0}_{-1.9}$	dynam	D
2MASS 1534-2952A	T4.5	1172 ± 79	51 ± 5	dynam	D
2MASS 1534-2952B	T5	1125 ± 79	48 ± 5	dynam	D
LSPM 1735+2634B	L0:	2274 ± 88	87 ± 3	dynam	D
Gl 758B (1923+3313)	T7:	581 ± 88	$37.9^{+1.4}_{-1.5}$	dynam	B
Gl 779B (2004+1704)	L4.5 ± 1.5	1533 ± 88	72.7 ± 0.8	dynam	B
Gl 802B (2043+5520)	[L5-L7]	1483 ± 88	66 ± 5	dynam	M
Gl 845B (2204-5646)	T1	1236 ± 79	75.0 ± 0.8	dynam	S
Gl 845C (2204-5646)	T6	965 ± 79	70.1 ± 0.7	dynam	S
2MASS 2244+2043	L6-8γ	1184 ± 10	10.46 ± 1.49	MovGp	F
DENIS 2252-1730A	[L4:]	1722 ± 134	59 ± 5	dynam	D
DENIS 2252-1730B	[T3.5]	1190 ± 79	41 ± 4	dynam	D

Notes. Legend for method: *MovGp* = mass comes from evolutionary models combined with the known age of the moving group or young association with which this object is a member; *dynam* = mass is measured dynamically. Reference code for mass determination: A = Brandt et al. (2020), B = Brandt et al. (2019), C = Climent et al. (2019), D = Dupuy & Liu (2017), F = Faherty et al. (2016), G = Gagné et al. (2017), H = Gagné et al. (2018b), I = Gagné et al. (2015a), M = Ireland et al. (2008), S = Dieterich et al. (2018), T = Dupuy et al. (2019), V = Garcia et al. (2017).

(This table is available in machine-readable form.)

5. Gl 229B: This object has an ultra-high mass for its effective temperature. Its measured mass is almost identical to that of Gl 845C, so the arguments for Gl 845C above also apply to Gl 229C. Brandt et al. (2020) note that an exceptionally old age for the Gl 229 system is disfavored, making Gl 229B another T dwarf whose mass measurement is at odds with expectations.

In summary, then, the masses expected from our simulations are consistent with the measured dynamical masses in Table 16 for most objects for which direct comparisons can be done. The exceptions are Gl 229B and Gl 845BC, which remain puzzles.

The consistency between most of the measurements and the expected values at higher masses gives us a cautious confidence—but not independent confirmation—in trusting model-implied values at lower masses. Of the 20 pc moving group members listed in Table 16, the ones of lowest mass are between 10 to 12 $M_{\rm Jup}$. So, within the 20 pc census, we are not able to push the cutoff mass below 10 $M_{\rm Jup}$ through either a critical analysis of the entire L, T, and Y sample nor through an analysis of the subset with moving group membership. Despite this limitation, we can look at the young moving group members in a larger sample volume, which strongly hint at a low-mass cutoff substantially below 10 $M_{\rm Jup}$. As discussed in Section 7.1, PSO J318.5338−22.8603, 2MASSW J1207334−393254b, and 2MASS J11193254−1137466AB are believed to have masses in the 4–7 $M_{\rm Jup}$ range, and other objects identified in Table 12 could possibly lower the limit within the 20 pc census itself.

9.3. The Age Distribution

We can also compare the expected age distributions with our limited knowledge of the ages for objects in the census. Figure 31 shows plots analogous to the mass distributions shown in Figure 30. For the Saumon & Marley (2008) evolutionary tracks in the 900–2250 K regime, the age distributions cover the entire range of 0–10 Gyr ages but with a skew toward young ages. The age distribution then flattens across the 600–900 K range, although the youngest ages

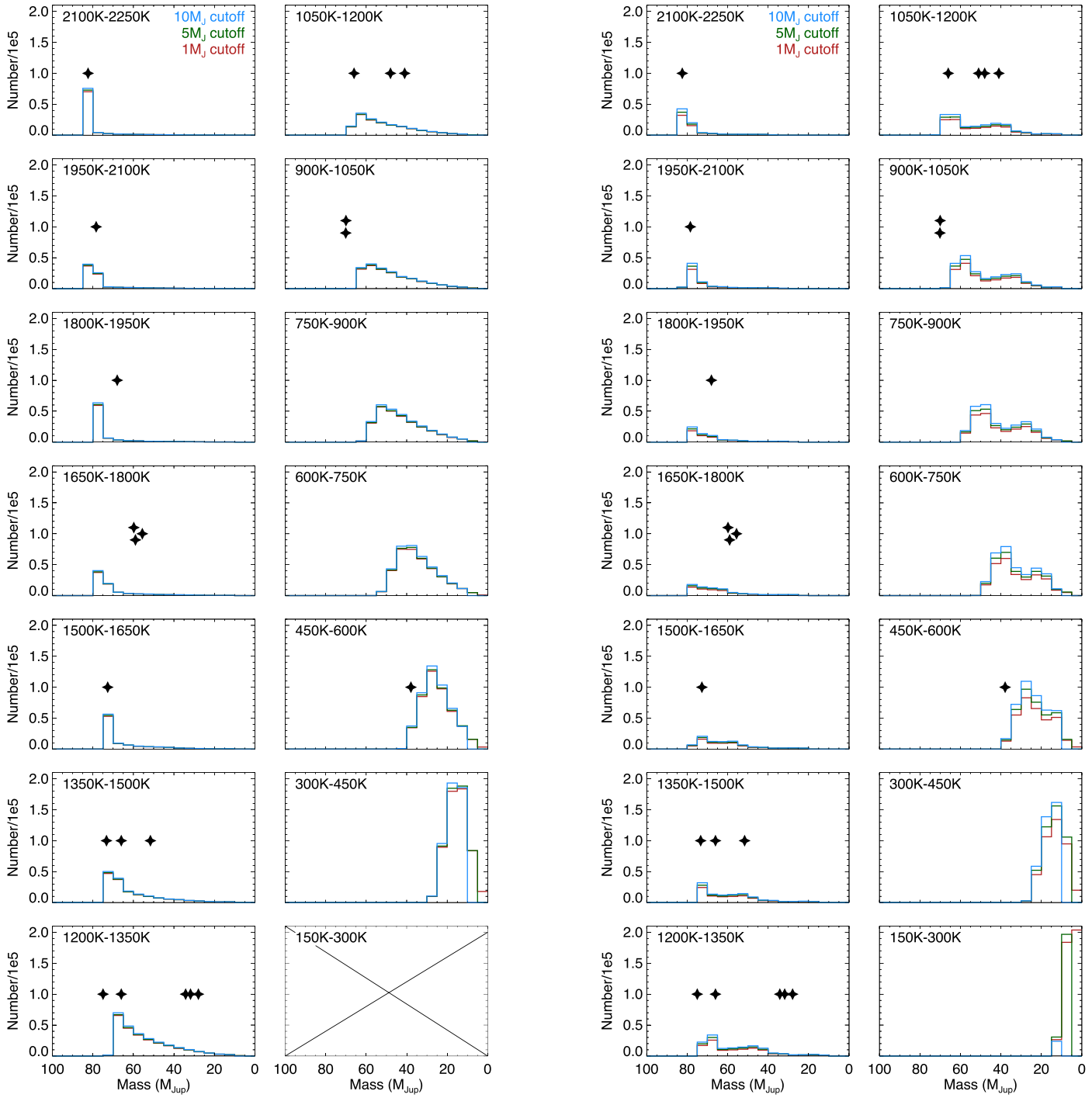

Figure 30. Simulated mass distributions for each of the 150 K $T_{\rm eff}$ bins. (a) The single power law of $\alpha = 0.5$ coupled with the Saumon & Marley (2008) evolutionary tracks. (b) The same, but coupled with the Baraffe et al. (2003) evolutionary tracks. Because the Saumon & Marley (2008) models do not extend below 300 K, the bin at lower right in panel (a) is empty. For ease of comparison, the same x and y scaling is used for all subpanels. Objects from Table 16 that have dynamically measured masses (filled black stars) are plotted in their $T_{\rm eff}$ bins at the x location corresponding to their mass; their y positions are arbitrary.

(<0.5 Gyr) start to disappear. A skew toward old ages appears below 600 K, with the skew becoming more severe with higher cutoff mass. The Baraffe et al. (2003) evolutionary tracks show that this skew toward old ages is exacerbated in the coldest bin (150–300 K). Here, a 10 $M_{\rm Jup}$ cutoff mass would imply no objects with ages <7 Gyr, whereas a 1 $M_{\rm Jup}$ cutoff would give a much more uniform age distribution, albeit with few objects having ages below 1 Gyr.

Most of the objects in the 20 pc L, T, and Y dwarf census lack age information, but we can examine this using tangential velocities as proxies of dynamical heating. Figure 32 shows the census' total proper motion and tangential velocity distributions. A total of 2% of the objects—nine in total—have $v_{\rm tan} > 100$ km s^{-1}. These objects are 2MASS 0251−0352 (112 km s^{-1}), 2MASS 0645–6646 (139 km s^{-1}), WISE 0833 +0052 (106 km s^{-1}), 2MASS 1126−5003 (127 km s^{-1}),

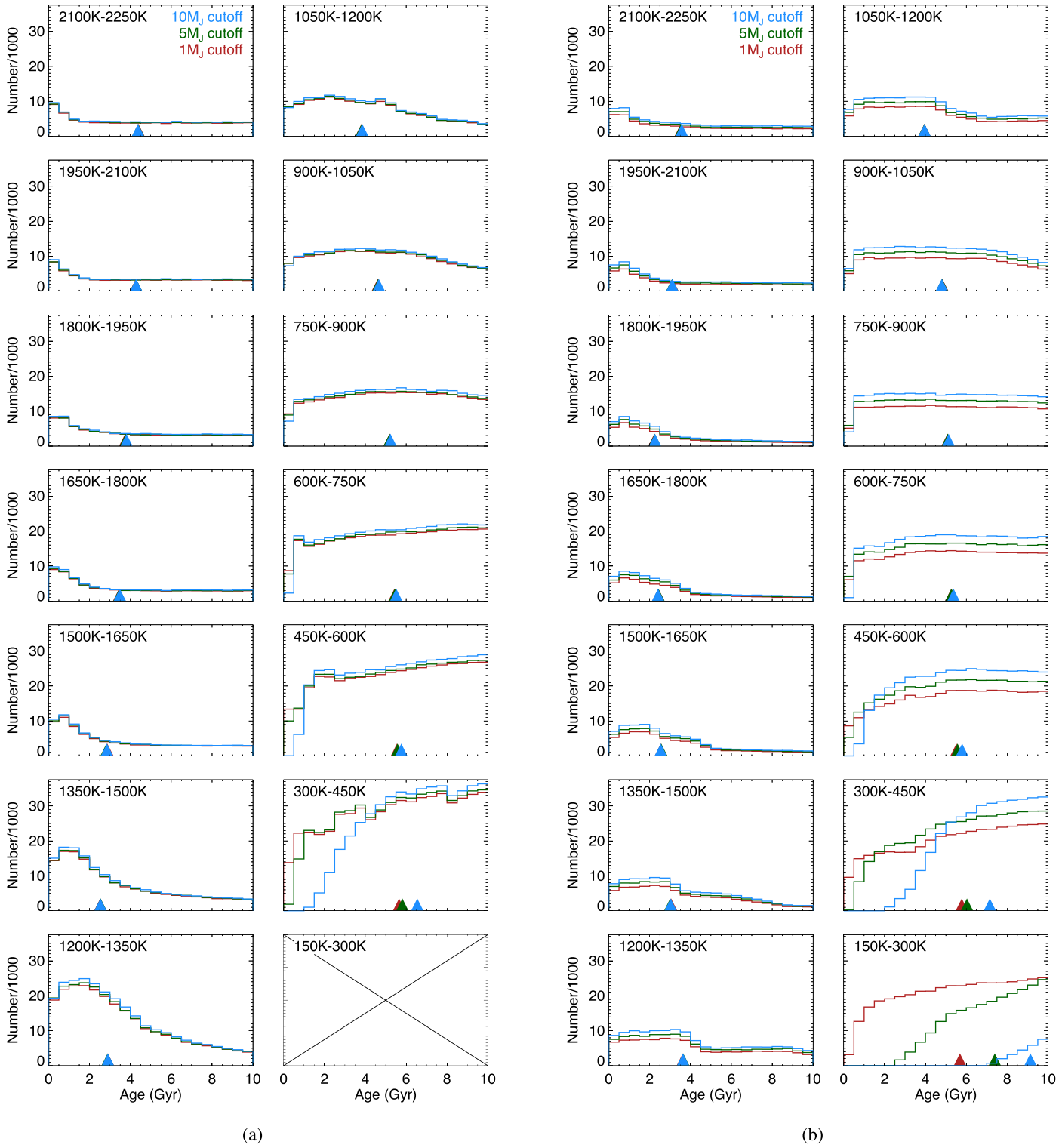

Figure 31. Simulated age distributions for each of the 150 K $T_{\rm eff}$ bins. (a) The single power law of $\alpha = 0.5$ coupled with the Saumon & Marley (2008) evolutionary tracks. (b) The same, but coupled with the Baraffe et al. (2003) evolutionary tracks. Because the Saumon & Marley (2008) models do not extend below 300 K, the bin in the lower right of panel (a) is empty. For ease of comparison, the same x and y scaling is used for all subpanels. The colored triangles along the bottom edge of each subpanel show the median age for cutoff masses of $10M_{\rm Jup}$ (blue), $5M_{\rm Jup}$ (green), and $1M_{\rm Jup}$ (red); these triangles overlap in all but the coldest bins.

2MASS 1231+0847 (106 km s^{-1}), DENIS 1253−5709 (128 km s^{-1}), 2MASS 1721+3344 (151 km s^{-1}), WISE 2005 +5424 (129 km s^{-1}), and Gl 802B (154 km s^{-1}). Three of these are subdwarfs discussed in Section 7.2, one is a possible subdwarf discussed in Section 7.6, two are blue/peculiar L dwarfs, and one is a companion to a mid-M binary believed to be ∼10 Gyr old (Ireland et al. 2008).

For the entire 20 pc census, we can check whether the expected inflation of the velocities at older ages is seen in our empirical data. To accomplish this, we compare the median

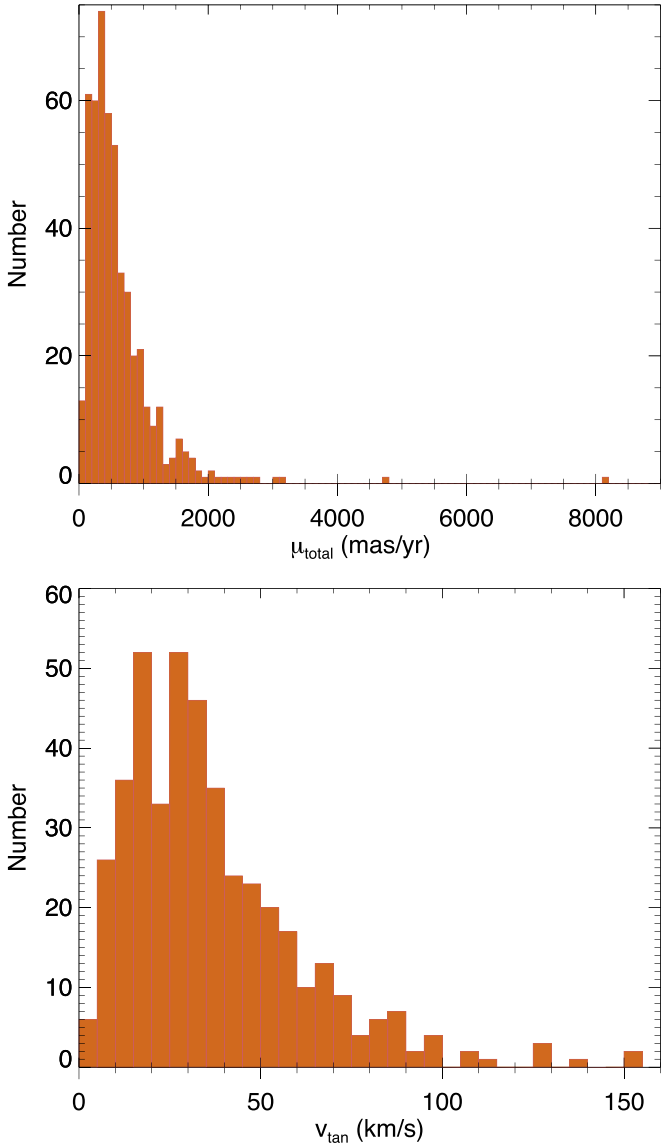

Figure 32. Histograms of the total proper motion and v_{tan} for the L, T, and Y dwarfs in the 20 pc census. In the upper diagram, the total motion is shown for all systems in the census. In the lower diagram, the tangential velocity is shown only for those systems having parallax measures with uncertainties below 12.5%. The median v_{tan} value for objects in the lower panel is 30.8 km s^{-1}.

ages expected from our simulations to the median v_{tan} values from our actual measurements. In Figure 31, we illustrate the median age at each 150 K bin for our $\alpha = 0.5$ power-law simulation. We also plot the measured tangential velocity against effective temperature in Figure 33, along with the median tangential velocity value in each of the 150 K bins. In Figure 31, we see that the median age shifts to younger values from 2250 K down to 1500 K and reaches a minimum in the 1350–1500 K bin before reversing course and trending to increasingly older values for increasingly cooler bins. Our measured v_{tan} values in Figure 33 show only a little variation across the 500–2250 K regime but increase substantially in the 300–450 K bin.

Although the agreement is qualitatively the same—in the sense that the colder, older objects have higher velocities indicative of dynamical heating—the coldest portion of our sample may be biased toward higher velocities anyway. Objects in the coldest bins are Y dwarfs that are uncovered

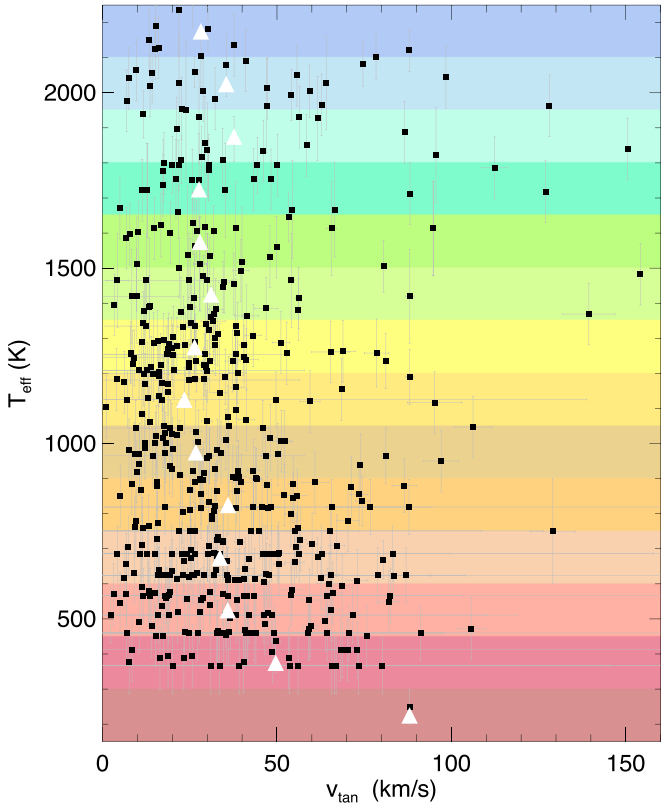

Figure 33. Tangential velocities plotted against effective temperature for L, T, and Y dwarfs in the 20 pc census. Only those objects having parallax measurements with uncertainties <12.5% are shown. Individual objects are shown as black squares, and the median v_{tan} values in each 150 K bin are shown as white triangles.

almost exclusively with WISE data and should have very red colors of W1−W2 > 4 mag. However, given their intrinsic faintness, they are usually not detected at W1, leading to W1 −W2 color limits only. As the W2 mags themselves grow fainter, this color limit becomes less useful, and thus a detection of proper motion is the best way to discern W2-only Y dwarfs from background chaff. This reliance on a proper motion signature—which at faint magnitudes is itself only reliable if the motion is large—leads to a kinematic bias. Thus, the larger median velocity in the 300–450 K bin may be a consequence of relying more heavily on motion as a selection criterion.

9.4. Where Are the WISE 0855−0714 Analogs?

In the next fainter bin, 150–300 K, WISE 0855−0714 is the only object recognized despite concentrated efforts to find other examples by both the Backyard Worlds and CatWISE teams. (With additional follow-up, WISE 0830+2837 from Bardalez Gagliuffi et al. (2020) may prove to be the second known member of this T_{eff} bin.) As Figure 31(b) demonstrates, objects in this bin should be heavily skewed toward older ages unless the low-mass cutoff is substantially less than 1M_{Jup}. Such a heavy skew to old ages also implies that such objects will be on average more metal-poor than the Sun.

It is possible that analogs to WISE 0855−0714 have already been cataloged in the thousands of faint motion candidates already identified by the Backyard Worlds and CatWISE teams but remain unrecognized? After all, many of the objects have W1−W2 color limits only and were never imaged by Spitzer to

provide more diagnostic ch1−ch2 colors. The answer is almost certainly "no," for the following reason. One of the criteria used to prioritize follow-up observations is the reduced proper motion, $H_{W2} = W2 + 5 \log \mu_{tot} + 5$, which is a crude measure of the object's intrinsic faintness based on its apparent magnitude and the size of its transverse motion. If any of the motion candidates lacking solid color had distinguished themselves with an exceptionally faint H_{W2} value—WISE 0855−0714 has $H_{W2} = 23.4$ mag (Figure 1 of Bardalez Gagliuffi et al. 2020)—it would certainly have been noticed. WISE 0830+2837 from Bardalez Gagliuffi et al. (2020), with $H_{W2} = 22.6$ mag, is the nearest contender now known.

Four possible scenarios to explain our lack of success in finding additional objects in the 150–300 K bin are: (1) they are exceedingly rare, (2) their intrinsic faintness places them too close to the W2 detection limit of WISE for motion searches to identify them confidently, (3) their motions are so high that coadds cannot be used to push the WISE detection limits deeper, and (4) their colors and magnitudes differ significantly from expectations. We discuss each of these scenarios below:

(1) The coldest objects are rare: Our result that the mass function is best fit with a power law of $\alpha = 0.6$ and that the cutoff mass is likely at or below $5M_{Jup}$ would imply a distribution of objects in the 150–300 K bin like that shown in the green curve in the lower right panel of Figure 31(b). This implies a space density of at least 2×10^{-3} pc^{-3}, which makes objects in this bin as common as T6 or T7 dwarfs. It is thus hard to reconcile these results with the hypothesis that such cold objects are extremely rare. Furthermore, it would be an unbelievable stroke of luck[55] that our Sun falls a mere 2.3 pc from such an extremely rare, cold object, as it does with WISE 0855−0714. Ergo, we reject rarity as a possible cause.

(2) WISE is too shallow: History has shown us that all-sky surveys can lead to curious results when researchers push those surveys near their limits. The bottom of the main sequence in the 1980s appeared to fall at late-M (Probst & Liebert 1983; Reid 1987) based on the dominant discovery engine of its time, the Palomar Observatory Sky Survey (Minkowski & Abell 1963; Reid et al. 1991). We now know, of course, that the reason for this is the low space density of early-L dwarfs (see Figure 29) and the fact that the POSS-I and POSS-II *B* and *R* plates failed to survey enough volume to detect all but the nearest L dwarf examples. The L/T pair WISE 1049−5319 is present on the southern UK Schmidt photographic plates but was not selected as a motion source (Luhman 2013); we find that Willem Luyten, despite having cataloged over 58,000 proper motion stars using photographic data (Luyten 1979), failed to catalog any of the 20 pc L dwarfs in Table 11. In the case of WISE, Wright et al. (2014) have used the relatively bright W2 magnitude of WISE 0855−0714 (W2 = 13.82 mag), its distance (2.3 pc), and the fact that it lies ∼2 mag above the limit of the AllWISE Catalog to argue that there should be another 4–35 similar objects already detected in AllWISE itself. The CatWISE Preliminary and CatWISE2020 Catalogs (see below) have increased the sensitivity to lower motions at fainter magnitudes, thus making the identification of these detected objects even easier. Hence, it is unlikely that the survey that found WISE 0855−0714 is too shallow to find other analogs.

(3) High motions confound deeper searches: The data sets using the longest time baseline of WISE data are CatWISE Preliminary (Eisenhardt et al. 2020) and CatWISE2020 (Marocco et al. 2020b). Most points on the celestial sphere are visited by WISE during a several-day window every six months. Both the CatWISE Preliminary and CatWISE2020 processing leveraged these repeats to measure proper motions of all sources. Full-depth coadditions, which took all of the available data to create a single, deep image, were used for source detection. Those source detections were then characterized through the stack of epochal coadds (from each six-month window) to measure photometry and astrometry for each source. Sources with significant proper motions could then be selected from the resulting source tables. Sources that fail to move a significant portion of a full-depth coadd's W2 FWHM (∼6″; Meisner et al. 2019) benefit from the coaddition, as their S/N increases by roughly the square root of the number of epochs. However, sources with higher motions do not see this benefit; a very high motion source will appear as a tracklet of separate sources in the full-depth coadd, and each separate apparition contains the background noise component from all epochs but the source signal from only one. Therefore, faint, high-motion sources can be lost in this process. If many of the coldest brown dwarfs are older kinematically, as Figures 31(a) and (b) suggest, their concomitant high proper motions may quash their identification by the CatWISE pipeline.

(4) Cold objects have unexpected colors or magnitudes: The analysis from Wright et al. (2014) inherently assumed that WISE 0855−0714 is a representative member of the Y dwarfs populating the 150–300 K bin. What if WISE 0855−0714 is atypical? It has $v_{tan} = 88.0$ km s^{-1}, which, although in the highest 4% of all v_{tan} values in Figure 33, is not exceptional. If the majority of objects in the 150–300 K bin are much older and have higher kinematics, then their high motions may suggest that point (3) above is a contributing cause. In addition, however, their older ages would also suggest a somewhat lower metallicity in general. If we look at the 20 pc T subdwarfs (Section 7.2) that have metallicity measurements, we find that values as low as $[M/H] = -0.3$ dex produce noticeable changes in the spectra of mid- to late-T dwarfs. Values of $[M/H] = -0.6$ dex begin to move objects into unfamiliar loci on color–magnitude diagrams. Inasmuch as molecular absorption strengths dictate the overall spectral energy distribution of Y dwarfs (Figure 15 of Doré et al. 2016), slight changes in metallicity could affect the relative importance of these bands and dramatically alter Y dwarf spectra and colors. Recent discoveries at early-T from Schneider et al. (2020) and A. M. Meisner et al. (private communication) underscore the point that warmer brown dwarfs with presumably lower metallicity ([Fe/H] ⩽ −1 dex) exist; their spectra are vastly different, at least in the near-infrared, from those of solar-metallicity T dwarfs. These may be harbingers of the photometric and spectroscopic bizarreness we can expect from the majority of later Y dwarfs, even if these Y dwarfs in general have less extreme metallicities.

In summary, other nearby objects with temperatures comparable to WISE 0855−0714 must exist, based on evidence from the mass function shape and knowledge of its low-mass cutoff. However, the expected higher motions and lower metallicities of objects in this 150–300 K bin may make

[55] It is already an oddity that our G star has, as its four closest neighbors, systems that harbor one G dwarf, one K dwarf, two M dwarfs, one L dwarf, one T dwarf, and one Y dwarf, since a random draw of the overall mass function would be heavily weighted toward M dwarfs plus a random K or T dwarf but weighted against rarer G or L dwarfs. See Kirkpatrick et al. (2012) for the full-sky 8 pc sample.

them a challenge to identify, especially when coupled with their intrinsic faintness.

10. Conclusions

Our results, which use the final trigonometric parallaxes we have measured using Spitzer, confirm the result of Kirkpatrick et al. (2019a) that the 20 pc brown dwarf portion of the mass function, which is based here on 525 L through Y dwarfs, can be best described as a power law with an exponent of $\alpha = 0.6 \pm 0.1$. We have not yet, however, extended this analysis to higher masses to investigate how the mass function behaves over the entire mass range within 20 pc. Earlier analyses have indicated that the higher-mass portion can be described as a two-part power-law (Kroupa et al. 2013) or log-normal form (Chabrier 2003a). New data, particularly data from Gaia DR2 and subsequent releases, can be used to refine our knowledge of the A through M dwarfs (and white dwarfs) with the 20 pc census as well as providing important astrometric information to help identify companions to those stars. Developing a database containing all knowledge of our stellar and substellar neighbors within this volume will enable us to explore the individual-object mass function with unprecedented detail.

Our results have also shown that the cutoff mass for star formation is constrained to be lower than $\sim 10 M_{\rm Jup}$ and that analysis of young moving group members over a wider sample likely constrains this value to $\sim 5 M_{\rm Jup}$. Obtaining a more solid value for the cutoff mass requires volume-complete subsets of a substantial number of Y dwarfs colder than 450 K, and particularly below ~350 K, a regime in which we have only one confirmed Y dwarf. Although WISE has provided a trove of Y dwarf discoveries, probing a substantial volume colder than ~350 K may require other resources. One such resource currently being planned is the Near Earth Object Surveyor (formerly called NEOCam) that is due to launch in 2025. As discussed in Kirkpatrick et al. (2019b), NEO Surveyor will cover 64% of the celestial sphere in two bands, NC1 and NC2, that cover wavelengths of 4.0–5.2 μm and 6.0–10.0 μm. Portions of the sky will be repeatedly scanned during their 75 day visibility windows, then scanned again roughly 215 days later when the next visibility window opens. The mission, although planned for five years, has a design lifetime of twelve years.

The absolute NC1 fluxes of a 350 K Y dwarf and a 250 K Y dwarf are 103 μJy and 26 μJy, respectively. The use of image differencing for high-motion objects in NEO Surveyor data will theoretically allow us to achieve single-epoch $S/N = 5$ sensitivities of ~4 μJy at NC1, thereby greatly increasing the distances to which we can detect these coldest brown dwarfs. However, NEO Surveyor is run through NASA's Planetary Defense Coordination Office, so no funding is being provided for the additional processing needed for astrophysical studies. For a relatively small investment, NASA Astrophysics could realize the full potential of NEO Surveyor data for stellar astrophysical research, of which cold brown dwarf discovery would be a major beneficiary.

This publication makes use of data products from WISE, which is a joint project of the University of California, Los Angeles, and the Jet Propulsion Laboratory (JPL), California Institute of Technology (Caltech), funded by the National Aeronautics and Space Administration (NASA). Work in this paper is based on observations made with the Spitzer Space Telescope, which is operated by JPL/Caltech, under a contract with NASA. Support for this work was provided to J.D.K. by NASA through a Cycle 14 award issued by JPL/Caltech. Some of the data presented here were obtained at the W. M. Keck observatory, which is operated as a scientific partnership among Caltech, the University of California, and NASA. The Observatory was made possible by the generous financial support of the W. M. Keck Foundation. The authors wish to recognize and acknowledge the very significant cultural role and reverence that the summit of Maunakea has always had within the indigenous Hawaiian community. We are most fortunate to have the opportunity to conduct observations from this mountain. Results here are partly based on observations obtained at the Hale Telescope, Palomar Observatory, as part of a continuing collaboration between Caltech, NASA/JPL, Yale University, and the National Astronomical Observatories of China. We would like to thank SURF students Tea Freedman-Susskind, Emily Zhang, Yerong Xu, and Feiyang Liu for help with the spectroscopic observation of WISE 2126+2530 from Palomar.

This work has made use of data from the European Space Agency (ESA) mission Gaia (https://www.cosmos.esa.int/gaia), processed by the Gaia Data Processing and Analysis Consortium (DPAC, https://www.cosmos.esa.int/web/gaia/dpac/consortium). Funding for the DPAC has been provided by national institutions, in particular the institutions participating in the Gaia Multilateral Agreement. This research has made use of IRSA, which is operated by JPL/Caltech, under contract with NASA. This research has also made use of the SIMBAD database, operated at CDS, Strasbourg, France. Federico Marocco acknowledges support from grant #80NSSC20K0452 under the NASA Astrophysics Data Analysis Program. Alfred Cayago gratefully acknowledges financial support through the Fellowships and Internships in Extremely Large Data Sets (FIELDS) Program, a National Aeronautics and Space Administration (NASA) science/technology/engineering/math (STEM) grant administered by the University of California, Riverside. Emily Martin is supported by an NSF Astronomy and Astrophysics Postdoctoral Fellowship under award AST-1801978. Eileen Gonzales acknowledges support from an LSSTC Data Science Fellowship. Christopher Theissen acknowledges support for this work through NASA Hubble Fellowship grant HST-HF2-51447.001-A awarded by the Space Telescope Science Institute, which is operated by the Association of Universities for Research in Astronomy, Inc., for NASA, under contract NAS5-26555. The Backyard Worlds: Planet 9 team thanks Zooniverse volunteers who have participated in the project. Backyard Worlds research was supported by NASA grant 2017-ADAP17-0067 and by the NSF under grants AST-2007068, AST-2009177, and AST-2009136. CatWISE is led by JPL/Caltech, with funding from NASA's Astrophysics Data Analysis Program. This research was partly carried out at JPL/Caltech, under contract with NASA. We thank the referee for a quick report despite difficulties imposed by the current pandemic.

Facilities: Spitzer(IRAC), WISE, Gaia, IRSA, CTIO:2-MASS, FLWO:2MASS, Blanco(NEWFIRM, ARCoIRIS), SO: Kuiper(2MASS), Gemini:South(FLAMINGOS-2), Magellan: Baade(PANIC, FIRE), FLWO:2MASS, Hale(WIRC, DBSP), SOAR(OSIRIS), DCT(NIHTS), Keck:II(NIRES), IRTF(SpeX), HST(WFC3).

Software: IDL (https://www.harrisgeospatial.com/Software-Technology/IDL), MOPEX/APEX (http://irsa.ipac.caltech.edu), mpfit (Markwardt 2009), WiseView (Caselden et al. 2018).

Appendix
Spectral Types, Astrometry, and Photometry for Systems

For systems in Tables 5–11, we have collected spectroscopic, astrometric, and photometric data from both this paper and the literature. These data are listed in Table A1. The various sections of the table are described in detail below. Close binaries are generally entered as a single entry with joint photometry unless there are components of the multiple with spectral types earlier than L0. For a full accounting of individual L, T, and Y components within the 20 pc census, refer to Table 11.

A.1. Origin and Name

Column *T* indicates the table(s) from which the source originates. Objects in the 20 pc census (Table 11) are indicated by "T." Users are encouraged to use this column, rather than the parallax column, if they wish to select the same set of objects that we included in our 20 pc census. Objects that are not listed in our 20 pc census (Table 11) but were nonetheless part of our Spitzer parallax program (Tables 5–7) are indicated by "P." Objects that are not from any of these tables but were part of our photometric or spectroscopic follow-up campaigns (Tables 8 and 9) are indicated by "F." Objects considered for the 20 pc census but ultimately not included (Table 10) are indicated by "C."

Column *ShortName* gives the abbreviated prefix and suffix of the full source name. This prefix is generally the survey of origin, and the abbreviated suffix is the sexagesimal R.A. and decl. of the source in the form $hhmm \pm ddmm$. As examples, CWISEP J193518.59−154620.3 is denoted as CWISE 1935−1546, and PSO J149.0341−14.7857 is denoted as PSO 0956−1447. Exceptions are made for objects with common names like Gl 570D and LHS 2397aB, whose full names are used instead.

A.2. Spectral Types

Columns *SpO* and *SpIR* list the optical and near-infrared spectral types, respectively, if known. These are converted to a decimal scale, and any qualifying criteria such as "pec," "β," and "sd" are dropped. The convention for the decimal scale is L0 = 0.0, T0 = 10.0, and Y0 = 20.0. As examples, an object with a spectral type of sdT8 is given as 18.0, and one with a type of L7: VL-G is given as 7.0. The two objects listed in Table 11 with types of "extremely red" in Mace et al. (2013a) are given in this table as 9.5. Column *SpAd* is the adopted spectral type, which is the same as *SpIR* if that value is not null; otherwise, it is the same as *SpO*. If both of those quantities are null, a spectral type estimate is given. A few objects, however, have null values for *SpAd*, and these are objects believed to be background interlopers and not brown dwarfs.

The source of the spectral type is given in column *OI*. An explanation of the double-letter code for this column can be found in the table comments.

A.3. Astrometric Data

Columns $\varpi_{\rm abs}$, μ_α, and μ_δ list the best measured trigonometric parallax and proper motion values in R.A. and decl. The "best" astrometry is simply that data set with the smallest quoted uncertainty in the parallax or, for objects lacking a parallax measurement, the data set with the smallest quoted uncertainty in the total proper motion. All parallaxes are given on the absolute reference grid; data from Tinney et al. (2003) and Tinney et al. (2014), along with USNO data from Kirkpatrick et al. (2019a), were converted from relative to absolute as described in Section 8 of Kirkpatrick et al. (2019a). The values listed for proper motion are a mixture of relative and absolute measurements. Readers are encouraged to cite the source of those values if this distinction is important for their research.

The source of the astrometry is given in column *AS*. An explanation of the single-letter code for this column can be found in the table comments.

A.4. JHK *Photometry*

Column J_{MKO} lists *J*-band photometry on the MKO system, $J_{\rm 2MASS}$ lists *J*-band photometry on the 2MASS system, *H* lists *H*-band photometry on either the MKO or 2MASS system, K_{MKO} lists *K*-band photometry on the MKO system, and $K_{S(\rm 2MASS)}$ lists K_S-band photometry on the 2MASS system. See Section 5.1.1 for details. Photometric values listed without corresponding errors are magnitude limits.

The source of the photometry is given in column *PhotS*. An explanation of the five-letter code for this column can be found in the table comments.

A.5. CatWISE2020 Data

Columns *RA_C2*, *Dec_C2*, *pmra_C2*, *pmdec_C2*, *W1mag_C2*, *W2mag_C2*, and *par_C2* contain astrometric information from the CatWISE2020 Catalog and Reject Table (Marocco et al. 2020b). The first two columns are the J2000 equinox R.A. and decl. positions from the moving-object solution at epoch MJD 57170.0, the next two columns are the measured proper motion and their uncertainties in R.A. and decl., the next two columns are the moving-object PSF-fit photometry in WISE bands W1 and W2, and the final column is a crude measurement of the object's parallax (called `par_pm` in the documentation).

The source of the CatWISE2020 data is given in column *C2S*. Upper-case "C2" refers to the Catalog and lower-case "c2" refers to the Reject Table.

A.6. AllWISE Data

Columns *W1mag*, *W2mag*, and *W3mag* provide stationary-object PSF-fit measurements (primarily from AllWISE) in WISE bands W1, W2, and W3. These are provided for two reasons. First, CatWISE2020 does not provide any W3 data, since this band was not available for the post-cryogenic phases of the WISE and NEOWISE missions. Second, the short, six-month time baseline of AllWISE means that this stationary-object photometry should be robust for all sources except those of exceptionally large motion, and thus the W1 and W2 photometry can be compared to the moving-object photometry from CatWISE2020 to provide another photometric check.

Table A1
Amassed Spectroscopic, Astrometric, and Photometric Data for Objects Listed in Tables 5–11

T	Name	SpO	SpIR	SpAd	OI	ϖ_{abs} (mas)	μ_α (mas yr^{-1})	μ_δ (mas yr^{-1})	AS	J_{MKO} (mag)	J_{2MASS} (mag)	H (mag)	K_{MKO} (mag)	$K_{S(2MASS)}$ (mag)	PhotS	RA_C2 (deg)	Dec_C2 (deg)	...
(1)	(2)	(3)	(4)	(5)	(6)	(7)	(8)	(9)	(10)	(11)	(12)	(13)	(14)	(15)	(16)	(17)	(18)	(19)
T	SDSS 0000+2554	15.0	14.5	14.5	TT	70.8 ± 1.9	−19.1 ± 1.5	126.7 ± 1.3	D	14.85 ± 0.01	15.06 ± 0.04	14.73 ± 0.07	14.82 ± 0.03	14.84 ± 0.12	U22D2	0.0563043	25.9054854	
T	GJ 1001BC	5.0	5.0	5.0	kT	82.0946 ± 0.3768	671.09 ± 0.35	−1498.16 ± 0.51	G	12.98 ± 0.01	13.11 ± 0.02	12.06 ± 0.03	⋯	11.39 ± 0.01	V22-V	1.1491771	−40.7415963	
T	WISE 0005+3737	⋯	19.0	19.0	−T	126.9 ± 2.1	997.3 ± 1.0	−271.6 ± 1.0	T	17.58 ± 0.04	⋯	17.98 ± 0.02	⋯	16.28 ± 0.31	U-k-2	1.3250452	37.6219054	
T	2MASS 0014−4844	2.5	2.5	2.5	TT	50.1064 ± 0.3898	870.72 ± 0.27	281.46 ± 0.43	G	13.91 ± 0.01	14.05 ± 0.04	13.26 ± 0.01	⋯	12.78 ± 0.01	V2V-V	3.7386552	−48.7367024	
T	WISE 0015−4615	⋯	18.0	18.0	−T	75.2 ± 2.4	413.4 ± 1.1	−687.8 ± 1.0	T	17.67 ± 0.02	⋯	17.91 ± 0.07	⋯	⋯	V-V–	3.7755685	−46.2558784	
T	2MASS 0015+3516	2.0	1.0	1.0	TT	58.6085 ± 0.3664	55.17 ± 0.45	−257.09 ± 0.28	G	13.71 ± 0.01	13.88 ± 0.03	12.89 ± 0.04	⋯	12.26 ± 0.02	UKK-2	3.9368016	35.2663391	

Notes. References for OI, where the reference for the optical (O) spectral type is given as the first character and that for the near-infrared (I) spectral type is given as the second character: (a) Albert et al. (2011), (A) Thompson et al. (2013), (b) Burningham et al. (2010), (B) Burgasser et al. (2010a), (c) Cushing et al. (2011), (C) Cushing et al. (2018), (d) Kirkpatrick et al. (2012), (D) Kirkpatrick et al. (2000), (e) Martin et al. (2018), (E) Reid et al. (2001a), (f) Kirkpatrick et al. (2010), (F) Faherty et al. (2014a), (g) Burgasser et al. (2006), (G) Bardalez Gagliuffi et al. (2014), (h) Hawley et al. (2002), (H) Dhital et al. (2011), (i) Chiu et al. (2006), (I) Koen et al. (2017), (J) Kirkpatrick et al. (1999), (j) Kirkpatrick et al. (2008), (k) Kirkpatrick et al. (2001), (K) Kirkpatrick et al. (2011), (l) Kendall et al. (2007), (L) Kendall et al. (2003), (m) Artigau et al. (2011), (M) Mace et al. (2013a), (n) Scholz et al. (2003), (N) King et al. (2010), (p) Potter et al. (2002), (P) Pineda et al. (2016), (q) Gizis (2002), (Q) Cruz et al. (2007), (r) Reid et al. (2008b), (R) Reid et al. (2006a), (s) Schneider et al. (2014), (S) Schneider et al. (2015), (t) Tinney et al. (2018), (T) See Tables 9–12 in this paper for references, (u) Burningham et al. (2013), (U) Burgasser (2007), (v) Schneider et al. (2017), (V) Kirkpatrick et al. (2016), (w) Kendall et al. (2004), (W) Best et al. (2013), (X) Burgasser et al. (2003a), (x) Thorstensen & Kirkpatrick (2003), (y) Deacon et al. (2014), (Y) Reylé et al. (2014), (z) Burgasser et al. (2010b), (Z) Fan et al. (2000). References for AS, the source of the astrometric data: (A) Dahn et al. (2002), (b) Burgasser et al. (2008b), (B) Bartlett et al. (2017), (c) CatWISE2020 Catalog, (C) Tinney et al. (2014), (d) Dahn et al. (2017), (D) Dupuy & Liu (2012), (E) Dupuy et al. (2019), (F) Faherty et al. (2012), (G) Gaia DR2—quoted astrometry is for the actual source listed, (g) Gaia DR2—quoted astrometry is that of the brighter primary in the system, (J) Kirkpatrick et al. (2011), (H) Hipparcos - van Leeuwen (2007), (K) Kirkpatrick et al. (2019a) for NTT and UKIRT parallaxes, (k) Kirkpatrick et al. (2019a) for USNO parallaxes, (l) Leggett et al. (2012), (L) Liu et al. (2016), (m) Manjavacas et al. (2013), (M) Marocco et al. (2010), (r) Smart, priv. comm., (R) Smart et al. (2018), (S) Casewell et al. (2008), (s) Smart et al. (2013), (t) Tinney et al. (2003), (T) This paper, (V) Vrba et al. (2004), (W) Best et al. (2020), (z) Dupuy et al. (2020), (Z) Lazorenko & Sahlmann (2018). References for PhotS, the source of the J, H, K photometry: (2) 2MASS Skrutskie et al. (2006), (a) Meisner et al. (2020a), (A) Meisner et al. (2020b), (b) Bardalez Gagliuffi et al. (2020) (Note that the HST F125W magnitude limit for WISE 0830+2837 is used as its value for J_{MKO}), (B) Bigelow/2MASS, (c) Boccaletti et al. (2003), (C) CTIO-4 m/NEWFIRM, (d) Kirkpatrick et al. (2012), (D) Database of Ultracool Parallaxes as of 2020 April: Dupuy & Liu (2012); Dupuy & Kraus (2013), and Liu et al. (2016), (e) Martin et al. (2018), (E) McElwain & Burgasser (2006), (f) Faherty et al. (2012), (F) Freed et al. (2003), (g) Mamajek et al. (2018), (G) Gemini-South/FLAMINGOS2, (h) Pinfield et al. (2014b), (H) Pinfield et al. (2014a), (i) Ireland et al. (2008), (I) Dupuy et al. (2019), (j) Janson et al. (2011), (J) Faherty et al. (2014b), (k) Kirkpatrick et al. (2019a), (K) Kirkpatrick et al. (2011), (m) Mace et al. (2013a), (M) Magellan/PANIC, (p) PAIRITEL, (P) Palomar/WIRC, (q) Dhital et al. (2011), (Q) Deacon et al. (2017b), (r) Deacon et al. (2012b), (s) Schneider et al. (2015), (S) SOAR/OSIRIS, (t) Tinney et al. (2014), (T) Thompson et al. (2013), (u) ULAS, UGPS, or UGCS, (U) UHS, (v) VVV, (V) VHS, (w) Wright et al. (2013), (W) Best et al. (2020). References for C2S, the source of the CatWISE2020 data: (C2) CatWISE2020 Catalog, (c2) CatWISE2020 Reject Table. References for WS, the source of the WISE photometry: (AW) AllWISE Source Catalog, (aw) AllWISE Reject Table, (C2) CatWISE2020 Catalog, (c2) CatWISE2020 Reject Table. References for SS, the source of the Spitzer photometry: (0) This paper, (f) Marocco et al. (2020a), (F) Filippazzo et al. (2015), (K) Kirkpatrick et al. (2019a), (L) Leggett et al. (2007), (M) Meisner et al. (2020a), (m) Meisner et al. (2020b), (P) Patten et al. (2006), (S) Metchev et al. (2015).

(This table is available in its entirety in machine-readable form.)

The source of the stationary-object photometry is given in column *WS*. In most cases, this is the AllWISE Source Catalog or Reject Table. Some sources, however, were not detected until `crowdsource` (Schlafly et al. 2018) was used on the unWISE images underlying the CatWISE2020 processing. In this case, the stationary-object W1 and W2 photometry from CatWISE2020 is listed instead.

A.7. Spitzer Data

Columns *ch1mag* and *ch2mag* provide the Spitzer channel 1 (3.6 μm) and channel 2 (4.5 μm) photometry. The source of this photometry is given in column *SS*, the single-character code for which is described in the table comments.

A.8. Note and Full Designation

Column *Note* lists a one-letter code indicating whether the object is an unresolved multiple (M); a young, low-gravity object (Y); or an old subdwarf (S). Column *FullName* gives the full discovery designation of the system.

ORCID iDs

J. Davy Kirkpatrick https://orcid.org/0000-0003-4269-260X
Jacqueline K. Faherty https://orcid.org/0000-0001-6251-0573
Aaron M. Meisner https://orcid.org/0000-0002-1125-7384
Dan Caselden https://orcid.org/0000-0001-7896-5791
Adam C. Schneider https://orcid.org/0000-0002-6294-5937
Federico Marocco https://orcid.org/0000-0001-7519-1700
R. L. Smart https://orcid.org/0000-0002-4424-4766
Marc J. Kuchner https://orcid.org/0000-0002-2387-5489
Edward L. Wright https://orcid.org/0000-0001-5058-1593
Michael C. Cushing https://orcid.org/0000-0001-7780-3352
Katelyn N. Allers https://orcid.org/0000-0003-0580-7244
Daniella C. Bardalez Gagliuffi https://orcid.org/0000-0001-8170-7072
Adam J. Burgasser https://orcid.org/0000-0002-6523-9536
Jonathan Gagné https://orcid.org/0000-0002-2592-9612
Sarah E. Logsdon https://orcid.org/0000-0002-9632-9382
Emily C. Martin https://orcid.org/0000-0002-0618-5128
James G. Ingalls https://orcid.org/0000-0003-4714-1364
Patrick J. Lowrance https://orcid.org/0000-0001-8014-0270
Ellianna S. Abrahams https://orcid.org/0000-0002-9879-1183
Eileen C. Gonzales https://orcid.org/0000-0003-4636-6676
Chih-Chun Hsu https://orcid.org/0000-0002-5370-7494
Nikita Kamraj https://orcid.org/0000-0002-3233-2451
Rocio Kiman https://orcid.org/0000-0003-2102-3159
Christopher Theissen https://orcid.org/0000-0002-9807-5435
Nikolaj Stevnbak Andersen https://orcid.org/0000-0003-4714-3829
Guillaume Colin https://orcid.org/0000-0002-7630-1243
Samuel J. Goodman https://orcid.org/0000-0003-2236-2320
Léopold Gramaize https://orcid.org/0000-0002-8960-4964
Leslie K. Hamlet https://orcid.org/0000-0002-7389-2092
Benjamin Pumphrey https://orcid.org/0000-0001-9692-7908
Austin Rothermich https://orcid.org/0000-0003-4083-9962
Arttu Sainio https://orcid.org/0000-0003-4864-5484
Melina Thévenot https://orcid.org/0000-0001-5284-9231

References

Aberasturi, M., Burgasser, A. J., Mora, A., et al. 2014, AJ, 148, 129
Aberasturi, M., Solano, E., & Martín, E. L. 2011, A&A, 534, L7
Adams, W. S. 1913, PASP, 25, 258
Adams, W. S., Joy, A. H., & Humason, M. L. 1926, ApJ, 64, 225
Adams, W. S., & Kohlschütter, A. 1914, CMWCI, 79, 1
Aganze, C., Burgasser, A. J., Faherty, J. K., et al. 2016, AJ, 151, 46
Albert, L., Artigau, É., Delorme, P., et al. 2011, AJ, 141, 203
Allen, P. R., Koerner, D. W., Reid, I. N., & Trilling, D. E. 2005, ApJ, 625, 385
Allers, K. N., & Liu, M. C. 2013, ApJ, 772, 79
Andrei, A. H., Smart, R. L., Penna, J. L., et al. 2011, AJ, 141, 54
Artigau, É., Doyon, R., Lafrenière, D., et al. 2006, ApJL, 651, L57
Artigau, É., Lafrenière, D., Doyon, R., et al. 2011, ApJ, 739, 48
Artigau, É., Radigan, J., Folkes, S., et al. 2010, ApJL, 718, L38
Baraffe, I., Chabrier, G., Barman, T. S., Allard, F., & Hauschildt, P. H. 2003, A&A, 402, 701
Bardalez Gagliuffi, D. C., Burgasser, A. J., Gelino, C. R., et al. 2014, ApJ, 794, 143
Bardalez Gagliuffi, D. C., Burgasser, A. J., Schmidt, S. J., et al. 2019, ApJ, 883, 205
Bardalez Gagliuffi, D. C., Faherty, J. K., Schneider, A. C., et al. 2020, ApJ, 895, 145
Bardalez Gagliuffi, D. C., Gagné, J., Faherty, J. K., et al. 2018, ApJ, 854, 101
Bardalez Gagliuffi, D. C., Gelino, C. R., & Burgasser, A. J. 2015, AJ, 150, 163
Barenfeld, S. A., Bubar, E. J., Mamajek, E. E., et al. 2013, ApJ, 766, 6
Bartlett, J. L., Lurie, J. C., Riedel, A., et al. 2017, AJ, 154, 151
Bastian, N., Covey, K. R., & Meyer, M. R. 2010, ARA&A, 48, 339
Batten, A. H. 1998, JRASC, 92, 231
Beamín, J. C., Minniti, D., Gromadzki, M., et al. 2013, A&A, 557, L8
Becklin, E. E., & Zuckerman, B. 1988, Natur, 336, 656
Bell, C. P. M., Mamajek, E. E., & Naylor, T. 2015, MNRAS, 454, 593
Bessel, F. W. 1838, MNRAS, 4, 152
Best, W. M. J., Liu, M. C., Dupuy, T. J., et al. 2017, ApJL, 843, L4
Best, W. M. J., Liu, M. C., Magnier, E. A., et al. 2013, ApJ, 777, 84
Best, W. M. J., Liu, M. C., Magnier, E. A., et al. 2015, ApJ, 814, 118
Best, W. M. J., Liu, M. C., Magnier, E. A., et al. 2020, AJ, 159, 257
Bihain, G., Scholz, R.-D., Storm, J., & Schnurr, O. 2013, A&A, 557, A43
Biller, B. A., Kasper, M., Close, L. M., Brandner, W., & Kellner, S. 2006, ApJL, 641, L141
Bloom, J. S., Starr, D. L., Blake, C. H., et al. 2006, in ASP Conf. Series 351, Astronomical Data Analysis Software and Systems XV, ed. C. Gabriel et al. (San Francisco: ASP), 751
Boccaletti, A., Chauvin, G., Lagrange, A.-M., et al. 2003, A&A, 410, 283
Borysow, A., Jorgensen, U. G., & Zheng, C. 1997, A&A, 324, 185
Bouy, H., Brandner, W., Martín, E. L., et al. 2003, AJ, 126, 1526
Bouy, H., Duchêne, G., Köhler, R., et al. 2004, A&A, 423, 341
Bouy, H., Martín, E. L., Brandner, W., et al. 2005, AJ, 129, 511
Bowler, B. P., Liu, M. C., & Dupuy, T. J. 2010, ApJ, 710, 45
Brandt, T. D., Dupuy, T. J., & Bowler, B. P. 2019, AJ, 158, 140
Brandt, T. D., Dupuy, T. J., Bowler, B. P., et al. 2020, AJ, 160, 196
Burgasser, A. J. 2001, PhD thesis, California Institute of Technology
Burgasser, A. J. 2004, ApJS, 155, 191
Burgasser, A. J. 2007, ApJ, 659, 655
Burgasser, A. J., Cruz, K. L., Cushing, M., et al. 2010a, ApJ, 710, 1142
Burgasser, A. J., Geballe, T. R., Leggett, S. K., Kirkpatrick, J. D., & Golimowski, D. A. 2006, ApJ, 637, 1067
Burgasser, A. J., Gillon, M., Melis, C., et al. 2015a, AJ, 149, 104
Burgasser, A. J., Kirkpatrick, J. D., Brown, M. E., et al. 1999, ApJL, 522, L65
Burgasser, A. J., Kirkpatrick, J. D., Brown, M. E., et al. 2002, ApJ, 564, 421
Burgasser, A. J., Kirkpatrick, J. D., Cutri, R. M., et al. 2000, ApJL, 531, L57
Burgasser, A. J., Kirkpatrick, J. D., Liebert, J., et al. 2003a, ApJ, 594, 510
Burgasser, A. J., Kirkpatrick, J. D., McElwain, M. W., et al. 2003b, AJ, 125, 850
Burgasser, A. J., Kirkpatrick, J. D., Reid, I. N., et al. 2003c, ApJ, 586, 512
Burgasser, A. J., Looper, D., & Rayner, J. T. 2010b, AJ, 139, 2448
Burgasser, A. J., Looper, D. L., Kirkpatrick, J. D., et al. 2007, ApJ, 658, 557
Burgasser, A. J., Looper, D. L., Kirkpatrick, J. D., et al. 2008a, ApJ, 674, 451
Burgasser, A. J., McElwain, M. W., & Kirkpatrick, J. D. 2003d, AJ, 126, 2487
Burgasser, A. J., McElwain, M. W., Kirkpatrick, J. D., et al. 2004, AJ, 127, 2856
Burgasser, A. J., Melis, C., Todd, J., et al. 2015b, AJ, 150, 180
Burgasser, A. J., Reid, I. N., Leggett, S. K., et al. 2005, ApJL, 634, L177
Burgasser, A. J., Sheppard, S. S., & Luhman, K. L. 2013, ApJ, 772, 129
Burgasser, A. J., Sitarski, B. N., Gelino, C. R., et al. 2011, ApJ, 739, 49
Burgasser, A. J., Tinney, C. G., Cushing, M. C., et al. 2008b, ApJL, 689, L53
Burningham, B., Cardoso, C. V., Smith, L., et al. 2013, MNRAS, 433, 457
Burningham, B., Lucas, P. W., Leggett, S. K., et al. 2011, MNRAS, 414, L90
Burningham, B., Pinfield, D. J., Leggett, S. K., et al. 2008, MNRAS, 391, 320
Burningham, B., Pinfield, D. J., Leggett, S. K., et al. 2009, MNRAS, 395, 1237

Burningham, B., Pinfield, D. J., Lucas, P. W., et al. 2010, MNRAS, 406, 1885
Burrows, A., Marley, M., Hubbard, W. B., et al. 1997, ApJ, 491, 856
Cardoso, C. V., Burningham, B., Smart, R. L., et al. 2015, MNRAS, 450, 2486
Casali, M., Adamson, A., Alves de Oliveira, C., et al. 2007, A&A, 467, 777
Caselden, D., Westin, P., Meisner, A., et al. 2018, WiseView: Visualizing motion and variability of faint WISE sources, Astrophysics Source Code Library, ascl:1806.004
Casewell, S. L., Jameson, R. F., & Burleigh, M. R. 2008, MNRAS, 390, 1517
Castro, P. J., Gizis, J. E., Harris, H. C., et al. 2013, ApJ, 776, 126
Chabrier, G. 2001, ApJ, 554, 1274
Chabrier, G. 2003a, PASP, 115, 763
Chabrier, G. 2003b, ApJL, 586, L133
Chauvin, G., Lagrange, A.-M., Dumas, C., et al. 2004, A&A, 425, L29
Chiu, K., Fan, X., Leggett, S. K., et al. 2006, AJ, 131, 2722
Clauset, A., Shalizi, C. R., & Newman, M. E. J. 2009, SIAMR, 51, 661
Climent, J. B., Berger, J. P., Guirado, J. C., et al. 2019, ApJL, 886, L9
Crundall, T. D., Ireland, M. J., Krumholz, M. R., et al. 2019, MNRAS, 489, 3625
Cruz, K. L., Kirkpatrick, J. D., & Burgasser, A. J. 2009, AJ, 137, 3345
Cruz, K. L., Reid, I. N., Kirkpatrick, J. D., et al. 2007, AJ, 133, 439
Cruz, K. L., Reid, I. N., Liebert, J., et al. 2003, AJ, 126, 2421
Cushing, M. C., Hardegree-Ullman, K. K., Trucks, J. L., et al. 2016, ApJ, 823, 152
Cushing, M. C., Kirkpatrick, J. D., Gelino, C. R., et al. 2011, ApJ, 743, 50
Cushing, M. C., Kirkpatrick, J. D., Gelino, C. R., et al. 2014, AJ, 147, 113
Cushing, M. C., Moskovitz, N., & Gustafsson, A. 2018, RNAAS, 2, 50
Cushing, M. C., Rayner, J. T., & Vacca, W. D. 2005, ApJ, 623, 1115
Cushing, M. C., Vacca, W. D., & Rayner, J. T. 2004, PASP, 116, 362
Dahn, C. C., Harris, H. C., Subasavage, J. P., et al. 2017, AJ, 154, 147
Dahn, C. C., Harris, H. C., Vrba, F. J., et al. 2002, AJ, 124, 1170
Dalton, G. B., Caldwell, M., Ward, A. K., et al. 2006, Proc. SPIE, 6269, 62690X
Day-Jones, A. C., Marocco, F., Pinfield, D. J., et al. 2013, MNRAS, 430, 1171
Deacon, N. R., Hambly, N. C., & Cooke, J. A. 2005, A&A, 435, 363
Deacon, N. R., Liu, M. C., Magnier, E. A., et al. 2011, AJ, 142, 77
Deacon, N. R., Liu, M. C., Magnier, E. A., et al. 2012a, ApJ, 757, 100
Deacon, N. R., Liu, M. C., Magnier, E. A., et al. 2012b, ApJ, 755, 94
Deacon, N. R., Liu, M. C., Magnier, E. A., et al. 2014, ApJ, 792, 119
Deacon, N. R., Magnier, E. A., Best, W. M. J., et al. 2017a, MNRAS, 468, 3499
Deacon, N. R., Magnier, E. A., Liu, M. C., et al. 2017b, MNRAS, 467, 1126
Delfosse, X., Tinney, C. G., Forveille, T., et al. 1997, A&A, 327, L25
Delorme, P., Delfosse, X., Albert, L., et al. 2008, A&A, 482, 961
Dhital, S., Burgasser, A. J., Looper, D. L., et al. 2011, AJ, 141, 7
Dieterich, S. B., Henry, T. J., Jao, W.-C., et al. 2014, AJ, 147, 94
Dieterich, S. B., Weinberger, A. J., Boss, A. P., et al. 2018, ApJ, 865, 28
Doré, O., Werner, M. W., Ashby, M., et al. 2016, arXiv:1606.07039
Doré, O., Werner, M. W., Ashby, M. L. N., et al. 2018, arXiv:1805.05489
Dupuy, T. J., & Kraus, A. L. 2013, Sci, 341, 1492
Dupuy, T. J., & Liu, M. C. 2012, ApJS, 201, 19
Dupuy, T. J., & Liu, M. C. 2017, ApJS, 231, 15
Dupuy, T. J., Liu, M. C., Best, W. M. J., et al. 2019, AJ, 158, 174
Dupuy, T. J., Liu, M. C., & Ireland, M. J. 2009, ApJ, 692, 729
Dupuy, T. J., Liu, M. C., & Leggett, S. K. 2015, ApJ, 803, 102
Dupuy, T. J., Liu, M. C., Magnier, E. A., et al. 2020, RNAAS, 4, 54
Dye, S., Lawrence, A., Read, M. A., et al. 2018, MNRAS, 473, 5113
Eikenberry, S., Elston, R., Raines, S. N., et al. 2006, Proc. SPIE, 6269, 626917
Eisenhardt, P. R. M., Marocco, F., Fowler, J. W., et al. 2020, ApJS, 247, 69
Ellis, S. C., Tinney, C. G., Burgasser, A. J., et al. 2005, AJ, 130, 2347
Emerson, J., McPherson, A., & Sutherland, W. 2006, Msngr, 126, 41
EROS Collaboration, Goldman, B., Delfosse, X., et al. 1999, A&A, 351, L5
Faherty, J. K., Beletsky, Y., Burgasser, A. J., et al. 2014a, ApJ, 790, 90
Faherty, J. K., Burgasser, A. J., Cruz, K. L., et al. 2009, AJ, 137, 1
Faherty, J. K., Burgasser, A. J., Walter, F. M., et al. 2012, ApJ, 752, 56
Faherty, J. K., Gagné, J., Burgasser, A. J., et al. 2018, ApJ, 868, 44
Faherty, J. K., Riedel, A. R., Cruz, K. L., et al. 2016, ApJS, 225, 10
Faherty, J. K., Tinney, C. G., Skemer, A., et al. 2014b, ApJL, 793, L16
Fan, X., Knapp, G. R., Strauss, M. A., et al. 2000, AJ, 119, 928
Fazio, G. G., Hora, J. L., Allen, L. E., et al. 2004, ApJS, 154, 10
Filippazzo, J. C., Rice, E. L., Faherty, J., et al. 2015, ApJ, 810, 158
Folkes, S. L., Pinfield, D. J., Jones, H. R. A., et al. 2012, MNRAS, 427, 3280
Folkes, S. L., Pinfield, D. J., Kendall, T. R., et al. 2007, MNRAS, 378, 901
Forveille, T., Ségransan, D., Delorme, P., et al. 2004, A&A, 427, L1
Francis, C. 2014, MNRAS, 444, L6
Freed, M., Close, L. M., & Siegler, N. 2003, ApJ, 584, 453
Gagné, J., Allers, K. N., Theissen, C. A., et al. 2018a, ApJL, 854, L27
Gagné, J., Burgasser, A. J., Faherty, J. K., et al. 2015a, ApJL, 808, L20
Gagné, J., Faherty, J. K., Burgasser, A. J., et al. 2017, ApJL, 841, L1
Gagné, J., Faherty, J. K., Cruz, K. L., et al. 2015b, ApJS, 219, 33
Gagné, J., Lafrenière, D., Doyon, R., et al. 2014, ApJ, 783, 121
Gagné, J., Mamajek, E. E., Malo, L., et al. 2018b, ApJ, 856, 23
Gaia Collaboration, Brown, A. G. A., Vallenari, A., et al. 2018, arXiv:1804.09365
Gaia Collaboration, Prusti, T., de Bruijne, J. H. J., et al. 2016, A&A, 595, A1
Garcia, E. V., Ammons, S. M., Salama, M., et al. 2017, ApJ, 846, 97
Gardner, J. P., Mather, J. C., Clampin, M., et al. 2006, SSRv, 123, 485
Gauza, B., Béjar, V. J. S., Pérez-Garrido, A., et al. 2015, ApJ, 804, 96
Geballe, T. R., Knapp, G. R., Leggett, S. K., et al. 2002, ApJ, 564, 466
Geißler, K., Metchev, S., Kirkpatrick, J. D., et al. 2011, ApJ, 732, 56
Gelino, C. R., Kirkpatrick, J. D., & Burgasser, A. J. 2004, AAS Meeting, 205, 11.13
Gelino, C. R., Kirkpatrick, J. D., & Burgasser, A. J. 2009, in AIP Conf. Proc. 1094, XV Cambridge Workshop on Cool Stars, Stellar Systems, and the Sun, 924
Gelino, C. R., Kirkpatrick, J. D., Cushing, M. C., et al. 2011, AJ, 142, 57
Gizis, J. E. 2002, ApJ, 575, 484
Gizis, J. E., Allers, K. N., Liu, M. C., et al. 2015a, ApJ, 799, 203
Gizis, J. E., Burgasser, A. J., & Vrba, F. J. 2015b, AJ, 150, 179
Gizis, J. E., Faherty, J. K., Liu, M. C., et al. 2012, AJ, 144, 94
Gizis, J. E., Monet, D. G., Reid, I. N., et al. 2000, AJ, 120, 1085
Gizis, J. E., Reid, I. N., Knapp, G. R., et al. 2003, AJ, 125, 3302
Gizis, J. E., Troup, N. W., & Burgasser, A. J. 2011, ApJL, 736, L34
Gliese, W. 1957, MiARI, 8, 1
Gliese, W. 1969, VeARI, 22, 1
Gliese, W., & Jahreiß, H. 1979, A&AS, 38, 423
Gliese, W., & Jahreiß, H. 1991, The Astronomical Data Center CD-ROM: Selected Astronomical Catalogs (Greenbelt, MD: Goddard Space Flight Center)
Goldman, B., Marsat, S., Henning, T., Clemens, C., & Greiner, J. 2010, MNRAS, 405, 1140
Golimowski, D. A., Henry, T. J., Krist, J. E., et al. 2004, AJ, 128, 1733
Gomes, J. I., Pinfield, D. J., Marocco, F., et al. 2013, MNRAS, 431, 2745
Gonzales, E. C., Faherty, J. K., Gagné, J., et al. 2019, ApJ, 886, 131
Gonzales, E. C., Burningham, B., Faherty, J. K., et al. 2020, ApJ, 905, 46
González-Fernández, C., Hodgkin, S. T., Irwin, M. J., et al. 2018, MNRAS, 474, 5459
Goto, M., Kobayashi, N., Terada, H., et al. 2002, ApJL, 567, L59
Greco, J. J., Schneider, A. C., Cushing, M. C., et al. 2019, AJ, 158, 182
Gustafsson, A., Moskovitz, N., Roe, H., et al. 2019, in EPSC-DPS Joint Meeting 2019, EPSC-DPS2019-1190
Hall, P. B. 2002, ApJL, 564, L89
Harrington, R. S., & Dahn, C. C. 1980, AJ, 85, 454
Hawley, S. L., Covey, K. R., Knapp, G. R., et al. 2002, AJ, 123, 3409
Henry, T. J., Jao, W.-C., Subasavage, J. P., et al. 2006, AJ, 132, 2360
Hertzsprung, E. 1907, Zeitschrift Fur Wissenschaftliche Photographie, 5, 86
Hertzsprung, E. 1922, BAN, 1, 21
Ingalls, J. G., Krick, J. E., Carey, S. J., et al. 2012, Proc. SPIE, 8442, 84421Y
Ireland, M. J., Kraus, A., Martinache, F., et al. 2008, ApJ, 678, 463
Janson, M., Carson, J., Thalmann, C., et al. 2011, ApJ, 728, 85
Kapteyn, J. C. 1903, Skew Frequency Curves in Biology and Statistics (Astronomical Laboratory, Groningen: Noordhoff)
Kasper, M., Biller, B. A., Burrows, A., et al. 2007, A&A, 471, 655
Kellogg, K., Kirkpatrick, J. D., Metchev, S., et al. 2018, AJ, 155, 87
Kellogg, K., Metchev, S., Gagné, J., et al. 2016, ApJL, 821, L15
Kellogg, K., Metchev, S., Geißler, K., et al. 2015, AJ, 150, 182
Kendall, T. R., Delfosse, X., Martín, E. L., et al. 2004, A&A, 416, L17
Kendall, T. R., Jones, H. R. A., Pinfield, D. J., et al. 2007, MNRAS, 374, 445
Kendall, T. R., Mauron, N., Azzopardi, M., et al. 2003, A&A, 403, 929
King, R. R., McCaughrean, M. J., Homeier, D., et al. 2010, A&A, 510, A99
Kirkpatrick, J. D. 2005, ARA&A, 43, 195
Kirkpatrick, J. D., Beichman, C. A., & Skrutskie, M. F. 1997, ApJ, 476, 311
Kirkpatrick, J. D., Cruz, K. L., Barman, T. S., et al. 2008, ApJ, 689, 1295
Kirkpatrick, J. D., Cushing, M. C., Gelino, C. R., et al. 2011, ApJS, 197, 19
Kirkpatrick, J. D., Cushing, M. C., Gelino, C. R., et al. 2013, ApJ, 776, 128
Kirkpatrick, J. D., Gelino, C. R., Cushing, M. C., et al. 2012, ApJ, 753, 156
Kirkpatrick, J. D., Henry, T. J., & McCarthy, D. W. 1991, ApJS, 77, 417
Kirkpatrick, J. D., Kellogg, K., Schneider, A. C., et al. 2016, ApJS, 224, 36
Kirkpatrick, J. D., Liebert, J., Cruz, K. L., et al. 2001, PASP, 113, 814
Kirkpatrick, J. D., Looper, D. L., Burgasser, A. J., et al. 2010, ApJS, 190, 100
Kirkpatrick, J. D., Martin, E. C., Smart, R. L., et al. 2019a, ApJS, 240, 19
Kirkpatrick, J. D., Metchev, S. A., Hillenbrand, L. A., et al. 2019b, BAAS, 51, 108

Kirkpatrick, J. D., Reid, I. N., Liebert, J., et al. 1999, ApJ, 519, 802
Kirkpatrick, J. D., Reid, I. N., Liebert, J., et al. 2000, AJ, 120, 447
Kirkpatrick, J. D., Schneider, A., Fajardo-Acosta, S., et al. 2014, ApJ, 783, 122
Kirkpatrick, J. D. 2003, in IAU Symp. 211, Brown Dwarfs, ed. E. Martín (San Francsico, CA: ASP), 189
Knapp, G. R., Leggett, S. K., Fan, X., et al. 2004, AJ, 127, 3553
Kniazev, A. Y., Vaisanen, P., Mužić, K., et al. 2013, ApJ, 770, 124
Koen, C., Miszalski, B., Väisänen, P., et al. 2017, MNRAS, 465, 4723
Koerner, D. W., Kirkpatrick, J. D., McElwain, M. W., et al. 1999, ApJL, 526, L25
Kroupa, P., Weidner, C., Pflamm-Altenburg, J., et al. 2013, in Planets, Stars and Stellar Systems, ed. T. D. Oswalt & G. Gilmore, Vol. 5 (Dordrecht: Springer Science+Business Media), 115
Kuchner, M. J., Faherty, J. K., Schneider, A. C., et al. 2017, ApJL, 841, L19
Kuiper, G. P. 1942, ApJ, 95, 201
Lang, D. 2014, AJ, 147, 108
Law, N. M., Hodgkin, S. T., & Mackay, C. D. 2006, MNRAS, 368, 1917
Lawrence, A., Warren, S. J., Almaini, O., et al. 2007, MNRAS, 379, 1599
Lazorenko, P. F., & Sahlmann, J. 2018, A&A, 618, A111
Leggett, S. K., Geballe, T. R., Fan, X., et al. 2000, ApJL, 536, L35
Leggett, S. K., Marley, M. S., Freedman, R., et al. 2007, ApJ, 667, 537
Leggett, S. K., Saumon, D., Marley, M. S., et al. 2012, ApJ, 748, 74
Leggett, S. K., Tremblin, P., Esplin, T. L., Luhman, K. L., & Morley, C. V. 2017, ApJ, 842, 118
Liebert, J., & Gizis, J. E. 2006, PASP, 118, 659
Liebert, J., Kirkpatrick, J. D., Cruz, K. L., et al. 2003, AJ, 125, 343
Limpert, E., Stahel, W. A., & Abbt, M. 2001, BioSc, 51, 341
Liu, M. C., Deacon, N. R., Magnier, E. A., et al. 2011, ApJL, 740, L32
Liu, M. C., Dupuy, T. J., & Allers, K. N. 2016, ApJ, 833, 96
Liu, M. C., Dupuy, T. J., Bowler, B. P., Leggett, S. K., & Best, W. M. J. 2012, ApJ, 758, 57
Liu, M. C., Dupuy, T. J., & Leggett, S. K. 2010, ApJ, 722, 311
Liu, M. C., Fischer, D. A., Graham, J. R., et al. 2002, ApJ, 571, 519
Liu, M. C., & Leggett, S. K. 2005, ApJ, 634, 616
Liu, M. C., Magnier, E. A., Deacon, N. R., et al. 2013, ApJL, 777, L20
Lodieu, N. 2020, MmSAI, 91, 84
Lodieu, N., Burningham, B., Day-Jones, A., et al. 2012, A&A, 548, A53
Lodieu, N., Pinfield, D. J., Leggett, S. K., et al. 2007, MNRAS, 379, 1423
Lodieu, N., Scholz, R.-D., & McCaughrean, M. J. 2002, A&A, 389, L20
Lodieu, N., Scholz, R.-D., McCaughrean, M. J., et al. 2005, A&A, 440, 1061
Looper, D. L., Gelino, C. R., Burgasser, A. J., et al. 2008a, ApJ, 685, 1183
Looper, D. L., Kirkpatrick, J. D., & Burgasser, A. J. 2007, AJ, 134, 1162
Looper, D. L., Kirkpatrick, J. D., Cutri, R. M., et al. 2008b, ApJ, 686, 528
Loutrel, N. P., Luhman, K. L., Lowrance, P. J., et al. 2011, ApJ, 739, 81
Lucas, P. W., Hoare, M. G., Longmore, A., et al. 2008, MNRAS, 391, 136
Lucas, P. W., Tinney, C. G., Burningham, B., et al. 2010, MNRAS, 408, L56
Luhman, K. L. 2013, ApJL, 767, L1
Luhman, K. L. 2014a, ApJL, 786, L18
Luhman, K. L. 2014b, ApJ, 781, 4
Luhman, K. L., Burgasser, A. J., & Bochanski, J. J. 2011, ApJL, 730, L9
Luhman, K. L., Loutrel, N. P., McCurdy, N. S., et al. 2012, ApJ, 760, 152
Luhman, K. L., Patten, B. M., Marengo, M., et al. 2007, ApJ, 654, 570
Luhman, K. L., & Sheppard, S. S. 2014, ApJ, 787, 126
Lutz, T. E., & Kelker, D. H. 1973, PASP, 85, 573
Luyten, W. J. 1979, New Luyten Catalog of Stars with Proper Motions Larger than Two Tenths of an Arcsecond (Minneapolis, MN: Univ. Minnesota)
Mace, G. N. 2014, PhD thesis, Univ. California, Los Angeles
Mace, G. N., Kirkpatrick, J. D., Cushing, M. C., et al. 2013a, ApJS, 205, 6
Mace, G. N., Kirkpatrick, J. D., Cushing, M. C., et al. 2013b, ApJ, 777, 36
Mace, G. N., Mann, A. W., Skiff, B. A., et al. 2018, ApJ, 854, 145
Mainzer, A., Bauer, J., Cutri, R. M., et al. 2014, ApJ, 792, 30
Mainzer, A., Cushing, M. C., Skrutskie, M., et al. 2011, ApJ, 726, 30
Malo, L., Doyon, R., Feiden, G. A., et al. 2014, ApJ, 792, 37
Mamajek, E. E., Marocco, F., Rees, J. M., et al. 2018, RNAAS, 2, 205
Manjavacas, E., Apai, D., Zhou, Y., et al. 2019, AJ, 157, 101
Manjavacas, E., Goldman, B., Reffert, S., & Henning, T. 2013, A&A, 560, A52
Markwardt, C. B. 2009, in ASP Conf. Series 411, Astronomical Data Analysis Software and Systems XVIII, ed. D. A. Bohlender et al. (San Francisco, CA: ASP), 251
Marocco, F., Andrei, A. H., Smart, R. L., et al. 2013, AJ, 146, 161
Marocco, F., Caselden, D., Meisner, A. M., et al. 2019, arXiv:1906.08913
Marocco, F., Jones, H. R. A., Day-Jones, A. C., et al. 2015, MNRAS, 449, 3651
Marocco, F., Kirkpatrick, J. D., Meisner, A. M., et al. 2020a, ApJL, 888, L19
Marocco, F., Smart, R. L., Jones, H. R. A., et al. 2010, A&A, 524, A38
Marocco, F., Eisenhardt, P. R. M., Fowler, J. W., et al. 2020b, ApJS, 253, 8
Martin, E. C., Kirkpatrick, J. D., Beichman, C. A., et al. 2018, ApJ, 867, 109
Martín, E. L., Delfosse, X., Basri, G., et al. 1999, AJ, 118, 2466
Martini, P., Persson, S. E., Murphy, D. C., et al. 2004, Proc. SPIE, 5492, 1653
McCaughrean, M. J., Close, L. M., Scholz, R.-D., et al. 2004, A&A, 413, 1029
McElwain, M. W., & Burgasser, A. J. 2006, AJ, 132, 2074
Meisner, A. M., Caselden, D., Kirkpatrick, J. D., et al. 2020a, ApJ, 889, 74
Meisner, A. M., Faherty, J. K., Kirkpatrick, J. D., et al. 2020b, ApJ, 899, 123
Meisner, A. M., Lang, D., Schlafly, E. F., et al. 2019, PASP, 131, 124504
Meisner, A. M., Lang, D., & Schlegel, D. J. 2018a, AJ, 156, 69
Meisner, A. M., Lang, D. A., & Schlegel, D. J. 2018b, RNAAS, 2, 202
Ménard, F., Delfosse, X., & Monin, J.-L. 2002, A&A, 396, L35
Metchev, S. A., Heinze, A., Apai, D., et al. 2015, ApJ, 799, 154
Metchev, S. A., Kirkpatrick, J. D., Berriman, G. B., et al. 2008, ApJ, 676, 1281
Metodieva, Y., Antonova, A., Golev, V., et al. 2015, MNRAS, 446, 3878
Miller, G. E., & Scalo, J. M. 1979, ApJS, 41, 513
Milligan, S., Cranton, B. W., & Skrutskie, M. F. 1996, Proc. SPIE, 2863, 2
Minkowski, R. L., & Abell, G. O. 1963, Basic Astronomical Data: Stars and Stellar Systems (Chicago, IL: Univ. Chicago Press), 481
Minniti, D., Lucas, P. W., Emerson, J. P., et al. 2010, NewA, 15, 433
Miret-Roig, N., Galli, P. A. B., Brandner, W., et al. 2020, A&A, 642, A179
Mróz, P., Udalski, A., Skowron, J., et al. 2017, Natur, 548, 183
Mugrauer, M., Seifahrt, A., Neuhäuser, R., & Mazeh, T. 2006, MNRAS, 373, L31
Murray, D. N., Burningham, B., Jones, H. R. A., et al. 2011, MNRAS, 414, 575
Nakajima, T., Oppenheimer, B. R., Kulkarni, S. R., et al. 1995, Natur, 378, 463
Nilsson, R., Veicht, A., Giorla Godfrey, P. A., et al. 2017, ApJ, 838, 64
Oke, J. B., & Gunn, J. E. 1982, PASP, 94, 586
Opitz, D., Tinney, C. G., Faherty, J. K., et al. 2016, ApJ, 819, 17
Patten, B. M., Stauffer, J. R., Burrows, A., et al. 2006, ApJ, 651, 502
Pecaut, M. J., & Mamajek, E. E. 2013, ApJS, 208, 9
Phan-Bao, N., Bessell, M. S., Martín, E. L., et al. 2008, MNRAS, 383, 831
Pineda, J. S., Hallinan, G., Kirkpatrick, J. D., et al. 2016, ApJ, 826, 73
Pinfield, D. J., Burningham, B., Lodieu, N., et al. 2012, MNRAS, 422, 1922
Pinfield, D. J., Burningham, B., Tamura, M., et al. 2008, MNRAS, 390, 304
Pinfield, D. J., Gomes, J., Day-Jones, A. C., et al. 2014a, MNRAS, 437, 1009
Pinfield, D. J., Gromadzki, M., Leggett, S. K., et al. 2014b, MNRAS, 444, 1931
Potter, D., Martín, E. L., Cushing, M. C., et al. 2002, ApJL, 567, L133
Prato, L., Mace, G. N., Rice, E. L., et al. 2015, ApJ, 808, 12
Pravdo, S. H., Shaklan, S. B., & Lloyd, J. 2005, ApJ, 630, 528
Probst, R. G., & Liebert, J. 1983, ApJ, 274, 245
Radigan, J., Jayawardhana, R., Lafrenière, D., et al. 2012, ApJ, 750, 105
Rayner, J. T., Toomey, D. W., Onaka, P. M., et al. 2003, PASP, 115, 362
Reid, I. N., Brewer, C., Brucato, R. J., et al. 1991, PASP, 103, 661
Reid, I. N., Burgasser, A. J., Cruz, K. L., et al. 2001a, AJ, 121, 1710
Reid, I. N., Cruz, K. L., Burgasser, A. J., et al. 2008a, AJ, 135, 580
Reid, I. N., Cruz, K. L., Kirkpatrick, J. D., et al. 2008b, AJ, 136, 1290
Reid, I. N., Gizis, J. E., Kirkpatrick, J. D., et al. 2001b, AJ, 121, 489
Reid, I. N., Kirkpatrick, J. D., Gizis, J. E., et al. 2000, AJ, 119, 369
Reid, I. N., Lewitus, E., Allen, P. R., et al. 2006a, AJ, 132, 891
Reid, I. N., Lewitus, E., Burgasser, A. J., et al. 2006b, ApJ, 639, 1114
Reid, N. 1987, MNRAS, 225, 873
Reylé, C. 2018, A&A, 619, L8
Reylé, C., Delorme, P., Artigau, E., et al. 2014, A&A, 561, A66
Riedel, A. R., Blunt, S. C., Lambrides, E. L., et al. 2017, AJ, 153, 95
Robert, J., Gagné, J., Artigau, É., et al. 2016, ApJ, 830, 144
Rojas-Ayala, B., Covey, K. R., Muirhead, P. S., et al. 2012, ApJ, 748, 93
Ruiz, M. T., Leggett, S. K., & Allard, F. 1997, ApJL, 491, L107
Salim, S., Lépine, S., Rich, R. M., et al. 2003, ApJL, 586, L149
Saumon, D., & Marley, M. S. 2008, ApJ, 689, 1327
Schlafly, E. F., Green, G. M., Lang, D., et al. 2018, ApJS, 234, 39
Schmidt, M. 1968, ApJ, 151, 393
Schmidt, S. J., Cruz, K. L., Bongiorno, B. J., et al. 2007, AJ, 133, 2258
Schmidt, S. J., West, A. A., Hawley, S. L., et al. 2010, AJ, 139, 1808
Schneider, A. C., Burgasser, A. J., Gerasimov, R., et al. 2020, ApJ, 898, 77
Schneider, A. C., Cushing, M. C., Kirkpatrick, J. D., et al. 2014, AJ, 147, 34
Schneider, A. C., Cushing, M. C., Kirkpatrick, J. D., et al. 2015, ApJ, 804, 92
Schneider, A. C., Greco, J., Cushing, M. C., et al. 2016, ApJ, 817, 112
Schneider, A. C., Windsor, J., Cushing, M. C., Kirkpatrick, J. D., & Shkolnik, E. L. 2017, AJ, 153, 196
Scholz, R.-D. 2010a, A&A, 510, L8
Scholz, R.-D. 2010b, A&A, 515, A92
Scholz, R.-D. 2020, A&A, 637, A45
Scholz, R.-D., & Bell, C. P. M. 2018, RNAAS, 2, 33

Scholz, R.-D., Bihain, G., Schnurr, O., & Storm, J. 2011, A&A, 532, L5
Scholz, R.-D., Bihain, G., & Storm, J. 2014, A&A, 567, A43
Scholz, R.-D., McCaughrean, M. J., Lodieu, N., & Kuhlbrodt, B. 2003, A&A, 398, L29
Scholz, R.-D., & Meusinger, H. 2002, MNRAS, 336, L49
Sengupta, S., & Marley, M. S. 2010, ApJL, 722, L142
Sheppard, S. S., & Cushing, M. C. 2009, AJ, 137, 304
Shkolnik, E. L., Allers, K. N., Kraus, A. L., et al. 2017, AJ, 154, 69
Simcoe, R. A., Burgasser, A. J., Bernstein, R. A., et al. 2008, Proc. SPIE, 7014, 70140U
Simcoe, R. A., Burgasser, A. J., Bochanski, J. J., et al. 2010, Proc. SPIE, 7735, 773514
Skrutskie, M. F., Cutri, R. M., Stiening, R., et al. 2006, AJ, 131, 1163
Smart, R. L., Bucciarelli, B., Jones, H. R. A., et al. 2018, MNRAS, 481, 3548
Smart, R. L., Marocco, F., Caballero, J. A., et al. 2017, MNRAS, 469, 401
Smart, R. L., Marocco, F., Sarro, L. M., et al. 2019, MNRAS, 485, 4423
Smart, R. L., Tinney, C. G., Bucciarelli, B., et al. 2013, MNRAS, 433, 2054
Smith, L., Lucas, P. W., Bunce, R., et al. 2014, MNRAS, 443, 2327
Strauss, M. A., Fan, X., Gunn, J. E., et al. 1999, ApJL, 522, L61
Subasavage, J. P., Jao, W.-C., Henry, T. J., et al. 2009, AJ, 137, 4547
Sumi, T., Kamiya, K., Bennett, D. P., et al. 2011, Natur, 473, 349
Swaters, R. A., Valdes, F., & Dickinson, M. E. 2009in ASP Conf. Series 411, Astronomical Data Analysis Software and Systems XVIII, ed. D. A. Bohlender et al. (San Francisco, CA: ASP), 506
Thalmann, C., Carson, J., Janson, M., et al. 2009, ApJL, 707, L123
Theissen, C. A., Bardalez Gagliuffi, D. C., Faherty, J. K., et al. 2020, RNAAS, 4, 67
Thompson, M. A., Kirkpatrick, J. D., Mace, G. N., et al. 2013, PASP, 125, 809
Thorstensen, J. R., & Kirkpatrick, J. D. 2003, PASP, 115, 1207
Tinney, C. G. 1998, MNRAS, 296, L42
Tinney, C. G., Burgasser, A. J., & Kirkpatrick, J. D. 2003, AJ, 126, 975
Tinney, C. G., Burgasser, A. J., Kirkpatrick, J. D., & McElwain, M. W. 2005, AJ, 130, 2326
Tinney, C. G., Faherty, J. K., Kirkpatrick, J. D., et al. 2012, ApJ, 759, 60
Tinney, C. G., Faherty, J. K., Kirkpatrick, J. D., et al. 2014, ApJ, 796, 39
Tinney, C. G., Kirkpatrick, J. D., Faherty, J. K., et al. 2018, ApJS, 236, 28
Tokunaga, A. T., Simons, D. A., & Vacca, W. D. 2002, PASP, 114, 180
Torres, S., Cai, M. X., Brown, A. G. A., et al. 2019, A&A, 629, A139
Tsuji, T., & Nakajima, T. 2003, ApJL, 585, L151
Tsvetanov, Z. I., Golimowski, D. A., Zheng, W., et al. 2000, ApJL, 531, L61
Vacca, W. D., Cushing, M. C., & Rayner, J. T. 2003, PASP, 115, 389
Valenti, J. A., & Fischer, D. A. 2005, ApJS, 159, 141
van Altena, W. F., Lee, J. T., & Hoffleit, D. 1995, yCat, 1174
van de Kamp, P. 1930, PA, 38, 17
van de Kamp, P. 1940, PA, 48, 297
van de Kamp, P. 1945, PASP, 57, 34
van de Kamp, P. 1953, PASP, 65, 73
van de Kamp, P. 1955, S&T, 14, 498
van de Kamp, P. 1969, PASP, 81, 5
van de Kamp, P. 1971, ARA&A, 9, 103
van Leeuwen, F. 2007, A&A, 474, 653
Volk, K., Blum, R., Walker, G., et al. 2003, IAUC, 8188, 2
Vrba, F. J., Henden, A. A., Luginbuhl, C. B., et al. 2004, AJ, 127, 2948
Warren, S. J., Mortlock, D. J., Leggett, S. K., et al. 2007, MNRAS, 381, 1400
Weinberger, A. J., Boss, A. P., Keiser, S. A., et al. 2016, AJ, 152, 24
West, A. A., Hawley, S. L., Bochanski, J. J., et al. 2008, AJ, 135, 785
Wilson, J. C., Eikenberry, S. S., Henderson, C. P., et al. 2003a, Proc. SPIE, 4841, 451
Wilson, J. C., Henderson, C. P., Herter, T. L., et al. 2004, Proc. SPIE, 5492, 1295
Wilson, J. C., Miller, N. A., Gizis, J. E., et al. 2003b, in IAU Symp. 211, Brown Dwarfs, ed. E. Martín (San Francisco, CA: ASP), 197
Winters, J. G., Henry, T. J., Lurie, J. C., et al. 2015, AJ, 149, 5
Wright, E. L., Eisenhardt, P. R. M., Mainzer, A. K., et al. 2010, AJ, 140, 1868
Wright, E. L., Mainzer, A., Kirkpatrick, J. D., et al. 2014, AJ, 148, 82
Wright, E. L., Skrutskie, M. F., Kirkpatrick, J. D., et al. 2013, AJ, 145, 84
Zapatero Osorio, M. R., Martín, E. L., Béjar, V. J. S., et al. 2007, ApJ, 666, 1205
Zhang, Z. H., Burgasser, A. J., Gálvez-Ortiz, M. C., et al. 2019, MNRAS, 486, 1260
Zhang, Z. H., Galvez-Ortiz, M. C., Pinfield, D. J., et al. 2018, MNRAS, 480, 5447
Zhang, Z. H., Pinfield, D. J., Gálvez-Ortiz, M. C., et al. 2017, MNRAS, 464, 3040
Zuckerman, B. 2019, ApJ, 870, 27
Zuckerman, B., Bessell, M. S., Song, I., et al. 2006, ApJL, 649, L115